Egyptian Journal of Geology, v. 63, 2019, p. 21-37

SHAPING BURIED BEDROCK TOPOGRAPHY USING RESISTIVITY AND GRAVITY DATA IN WADI ALLAQI, EASTERN DESERT, EGYPT

Ahmad Sobhy Helaly

Department of Geophysics, Faculty of Science, Ain Sham University, Cairo, Egypt. 11566
E-mail: Ahmad.Helaly@sci.asu.edu.eg

ABSTRACT

Vertical electrical resistivity and Bouguer gravity data were assessed at Wadi Allaqi area, Eastern Desert, Egypt aiming at the configuration of the bedrock (basement) surface, potential of groundwater availability and assessment ofthe best locations for drilling groundwater boreholes.

The results obtained from geoelectrical resistivity interpretation have shown that the interpreted depths of basement surface range from about five m to sixty m with three main deeper troughs considered as best locations for groundwater accumulation and suitable for drilling of groundwater boreholes. Since, the gravity anomaly magnitude is mainly controlled by the depth to the subsurface causative feature (basement) and its density contrast with overburden. Many trials for estimating the depth at varying density contrasts (0.1-1.0 gm/cm^3) were done. It is found that the closest depths from the gravity analysis to the obtained resistivity analysis are the ones that were computed using the density contrast of 0.2 gm/cm^3 as an optimum value. Finally, re-mapping bedrock topography based on that optimum value was achieved.

Keywords: Bedrock Topography, VES, Gravity, Density Contrast, Detailed Residual.

INTRODUCTION

One of the important mechanisms that shape the topographic features is the erosion of bedrock; that links climatic and tectonic processes. The quantity of sediments covering bedrock is an important control on the groundwater potentiality in any area. The use of geophysical methods for both groundwater resources mapping and water quality evaluation has increased dramatically over the last decades due to rapid advances in electronic technology and the development of numerical modeling solutions (Olayinka, 1991, Metwaly et al., 2009 and Ndlovu et al., 2010). Therefore, we need to evaluate the quantity of sediment covering bedrock through estimating of the contact between the sediments and the bedrock which is an important factor for exploring the volume of sediment in river bottoms. Using nondestructive geophysical investigation techniques, such as geoelectrical resistivity surveys and gravity methods, we can quantify the magnitude and variability of sediment covering bedrock faster, cheaper, and over a broader area than drilling a well or digging a trench. Gravimetric method can be used as a method of low cost, can be used in areas with enough contrasting density, such as between the weathered overburden and the bedrock (Telford and Sheriff, 1990). Geoelectric resistivity of subsurface rocks is also one of the variables which affect the physical properties of the rock layers below the surface. Rock resistivity data can be used to develop a model of subsurface and stratigraphic structures in terms of geoelectrical properties, which depends on lithology, air/water content, porosity, and pore ions concentration...etc.

The study area, named Wadi Allaqi lies within the Longitudes 33º08'E & 33º21'E and Latitudes 22º36'N & 22º46'N, in thesoutheastern region of Eastern Desert in Egypt as shown in the location map **(**Fig. 1).

To realize the potential of water availability, geophysicalfield data were studiedtargetingthe configuration of the bedrock in the study area for its assessment ofthe groundwater availability in the aquiferous horizonwithin the study area and siting the best possibleboreholes locations for groundwater extraction.

GEOLOGIC SETTING

Geomorphologically,the study area is occupied by a number of valleys and is surrounded by mountains and highlands composed of complex basement rocks. Such valleys are mostly plains covered with sands, gravels and rock fragments. These valleys are gently sloping towards the southeast. From field observations, it is found that the deposited layers are also dipping towards the southeast.

Geologically, Wadi Allaqi is one of the most important valleys in the southern part of the Eastern Desert, to the east of Naser Lake.This valley is filled with fluvial sand and silt deposits belonging to Quaternary (Pleistocene) age. Figure (2) shows a geological map illustrating that Wadi Allaqi is bounded by igneous and metamorphic rocks from the east, while from the west, it is bounded by Nubian Sandstone.

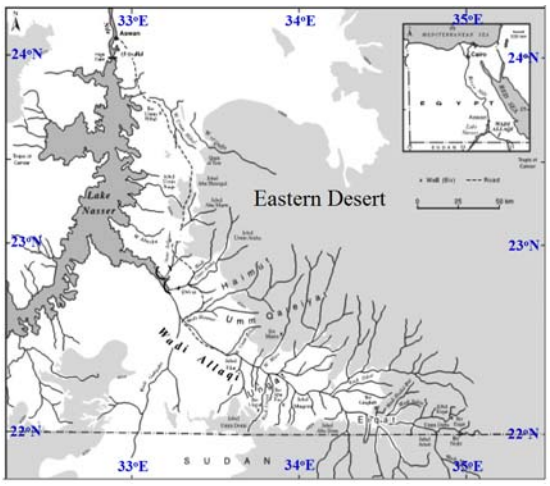

Fig. 1: General location map of the study area & surroundings (Kandal et al, 2016).

More enlightening information about the geology of the study area and its surroundings points to that, in general, about 50% of the granitic rocks in the Eastern Desert are classified as older and younger granites. The younger granites cover about 30% of the plutonic rocks in the Arabian shield. The relative abundance of the younger granites compared to the older granites increases from 1:4 due south of the Eastern Desert to about 1:1 due north (Stern and Hedge, 1985). The hilly areas surrounding Wadi Allaqi (Gabal Abu Marw, Gabal Haumor and Gabal um Shalman) are related to the younger granite and late organic granite (El-Shazly, 1964). (The word "Gabal" is the Arabic word for mountain). These granites are younger than the surrounding country rocks represented by meta-sediments, meta-volcanic and meta-gabbro rocks.

The general geologic map of Wadi Allaqi area and surrounding areas is shown in Figure (2).The rock varieties encountered from the oldest to the youngest are serpentines, talc carbonate, meta-sediments, meta-volcanic, metagabbro, gabbro, diorite granodiorite and Quaternary wadi deposits. This is with shear zone-associated auriferous quartz veins within ophiolitic-island arc metavolcanic terrains.

Also, Zoheir and Emam, (2012) compiled the geological and structural elements exposed in the mining sites within the Wadi Allaqi region, from integrated field, petrographic and satellite imagery data analysis.A highly tectonized, strongly foliated NW–SE-trending belt of interlayered ophiolitesand island arc metavolcanic/volcaniclastic rocks dominates the area. This belt is cut by sheared and non-deformed granitoids intrusions. The ophiolitic rocks include serpentinite, metagabbro, metabasalt, and their highly sheared and metasomatized derivatives. The contact zone between metagabbro and serpentinite is defined by steeplydipping thrust structures, locally imposed by tight to isoclinal folds.

The study area (and its surroundings) subjected to several phases of deformations expressed by superimposed structures, including from older to younger:

(1) WNW-trending folds and antiforms and related foliations, commonly developed in the island arc metavolcanic rocks;

(2) NW- to NNW-trending, overturned folds and steeply-dipping, SE-vergent thrust segments and crenulation cleavage, common in ophiolitic rocks; and

(3) NNW-trending shear and mylonitic zones, quartz pods, conjugate sinistral NNW–SSE and dextral WNW–ESE strike-slip faults in the island arc and ophiolitic rocks everywhere in the study area and its surroundings.

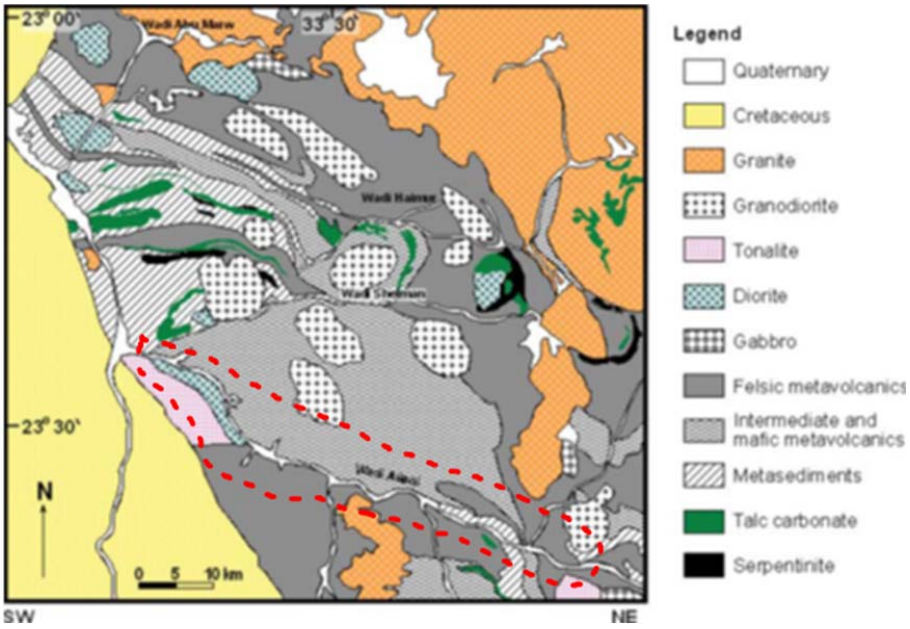

Fig. 2: Geological map of the study area (Wadi Allaqi)(Shams et al, 2012)

The subsurfacegeologic setup was recently described by Khedr, et al. (2010) through their study of the stratigraphic rock units in and around Wadi Allaqi (Fig. 3). Khedr, et al. (2010) suggested one formal "Group" of formation called the "***Nubia Group***". The clastic sequence which took place over the hard basement rocks including two un-official names of stratigraphic Groups or clusters of formations either underneath the Nubia Group (***Infra***) or overlying the Nubia Group (***Ultra***).

1) The ***Infra Nubia Group*** includes all clastic rocks laid over the basement hard-rocks or their weathered zone. It represents sedimentary rocks ranging in age between Cambrian and pre-Late Jurassic age. This division includes four Paleozoic Formations, from base upward these are: Araba Fm.,Gbgaba Fm., Naqus Fm., and Wadi Malik Fm. It also included the so called Abu Aggag Formation. The Infra Nubia sequence belongs to Ordovician-Silurian age and is made up of 400m thick undisturbed and recycled glacio-fluvial sands and gravels, exposed near Gebel Uwainat at the southwestern corner of Egypt.

2) The***Nubia Group*** rock unit of Late Jurassic-Maastrichtian age and includes the Abu Ballas Formation, Taref Sandstone, Quseir Formation and covered by the "Maastrichtian-Recent" Ultra Nubia Group which started over the top of the Nubian Sandstone.

3) The ***Ultra Nubia Group*** which includes all stratigraphic formations which took place since the early Paleocene and extends until the present time. The ***Ultra Nubia Group*** includes the Dakhla Formation, Esna Formation at the eastern bank of the Nile together with the coeval Paleocene age Kurkur and Garra Formations in the western side of the Nile as well as the followed upwards stratigraphic-formations in the study area.

GEOPHYSICAL WORK

Among the geophyical techniques that play crucial role in search for appropriate groundwater resources are the geoelectrical resistivity and gravity techniques. The two techniques have been used tremindously for that specific purpose.

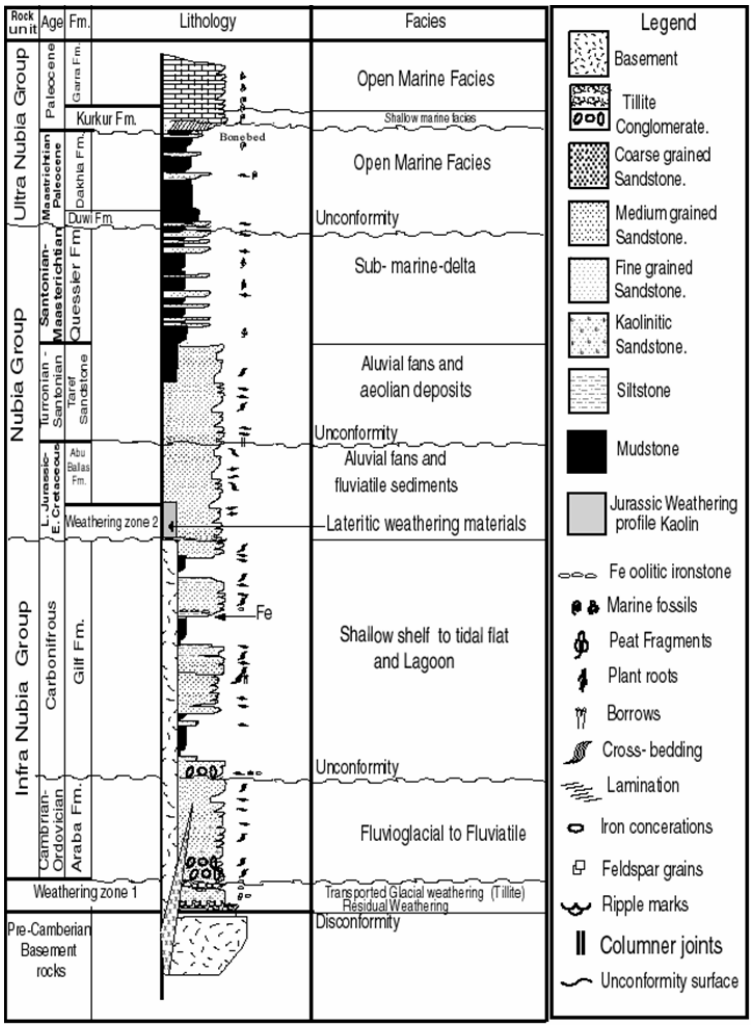

Fig. 3: Generalized stratigraphic column of the study area (Khedr et al, 2010)

GEOELECTRICAL RESISTIVITY TECHNIQUE

Forty vertical electrical soundings (40 VES's) have been used for the current study, where their relative geographic locations are shown in Figure (4). The well known Schlumberger configuration was used in the field work, where the two outer electrodes (AB) together with the two inner electrodes (MN) were kept colinear and the M-N spacing was kept equal or less than the 1/5 of A-B spacing during the survey work. The maximum AB/2 spacing was 200 meters. Most of the surveyed probes are located within the main valley, while other probes were also within the secondary surrounding tributaring valleys.

The measured apparent resistivity versus current electrode spacing data taken at each location are illustrated in Figure (5). Such data were then analyzed qualitatively in terms of varying number of layers and their relative varying measured apparent resistivity. The combinations of the illustrated VES's showed various mostly three-, and four-layer curves.

Almost all measured VES's were ended up by an increasing measured apparent resistivity. That indicates the below-lying bedrock is of crystalline nature, probably like the volcanics and metasediments characterized by very low electrical conductivity and higher resistivity than the overlying overburden. This is followed by the quantitative interpretation of these VES's which was mainly to determine the thickness of the overburden overlying the below-lying bedrock, and hence, determining the depth to the underlying bedrock. Existing groundater potentiality in the study area was then deduced based on such results.

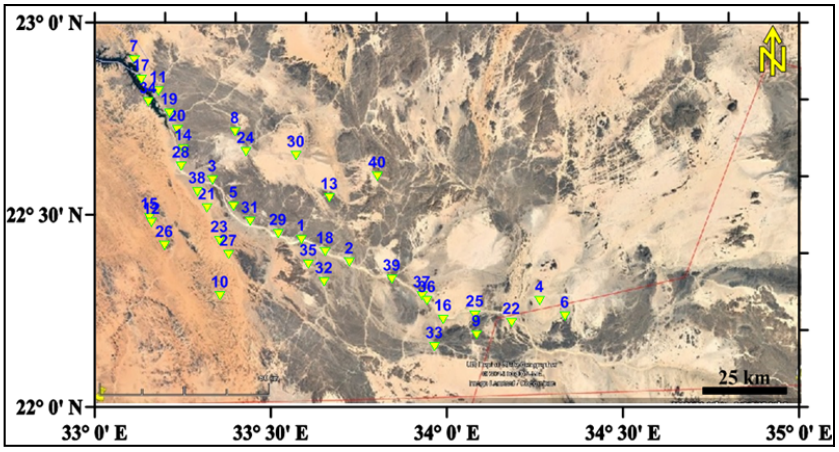

Fig. 4: VES's location and numbers superimposed on satellite map

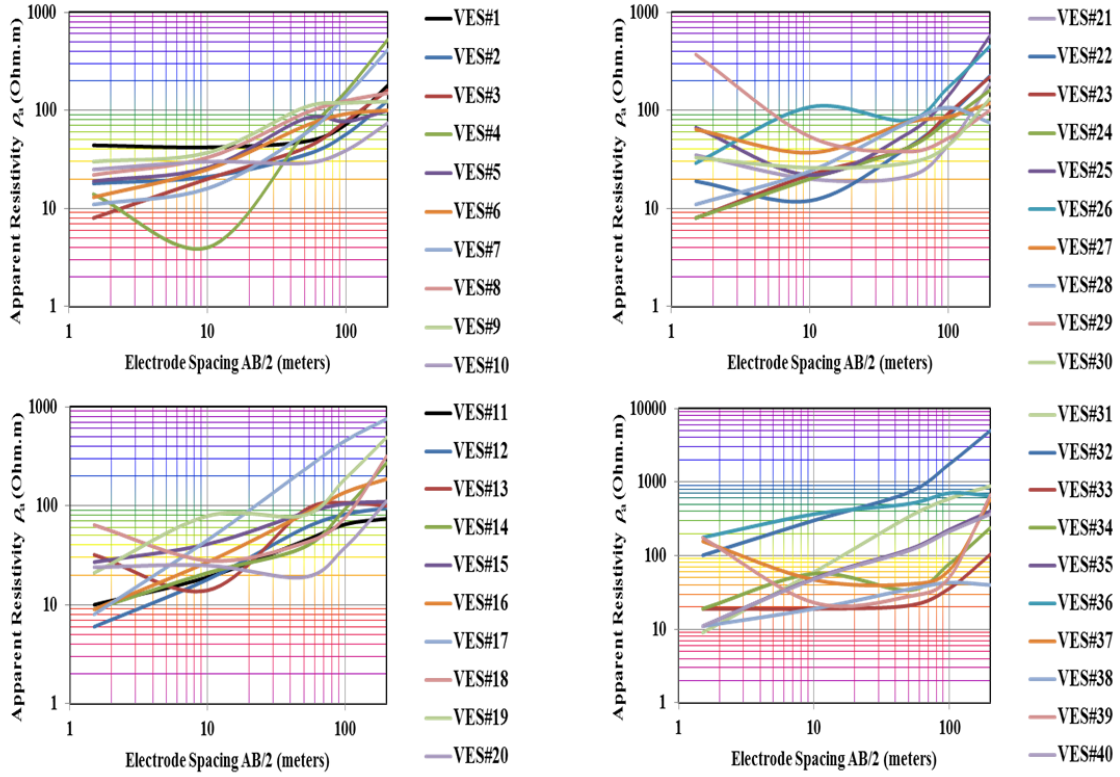

Fig. 5: Collective representation of the used VES's (AB/2 vs ρ_a)

Almost all measured VES's were ended up by an increasing measured apparent resistivity. That indicates the below-lying bedrock is of crystalline nature, probably like the volcanics and metasediments characterized by very low electrical conductivity and higher resistivity than the overlying overburden. This is followed by the quantitative interpretation of these VES's which was mainly to determine the thickness of the overburden overlying the below-lying bedrock, and hence, determining the depth to the underlying bedrock. Existing groundater potentiality in the study area was then deduced based on such results.

For the needed qualitative interpretation, a long profile through the main valley path segmented into two profiles were done. The first profile (Fig. 6) is passing through the VES's (West) 7, 17, 11,19,20,14,28,3,5 and 31 (East). The second profile (Fig. 7) runs through the VES's (West) 29, 1, 18, 2, 39, 37, 36, 16, 25 and 22 (East).

Figure (6A) shows the amount of fitting error in pseudo cross-section. It shows that for the most of the studied VES's along this profile, the fitting error is ranging within 5% or less. Except in some VES's like

VES's 17, 19, 20, and 14 – the error was about 10-15% at depths of units at an approximate depths of about 50 meters. Figure (6B), shows the pseudo cross-section (above) and a corresponding resistivity cross-section (below). Higher resistive deeper horizons were detected deeper below VES's 17, 19, 20, and 14 at shallower depths than at the eastern side of the first profile. Figure (6C) represents the relative electrical conductance along this profile which shows the conductance used in the resistivity cross-section down to a a certain depth below each VES. It varies from 0.2 to 0.7. As shown, the majority of the deeper zones within the resistivity cross-section is dominated by higher resistive blocks representing the deeper-seated bedrock.

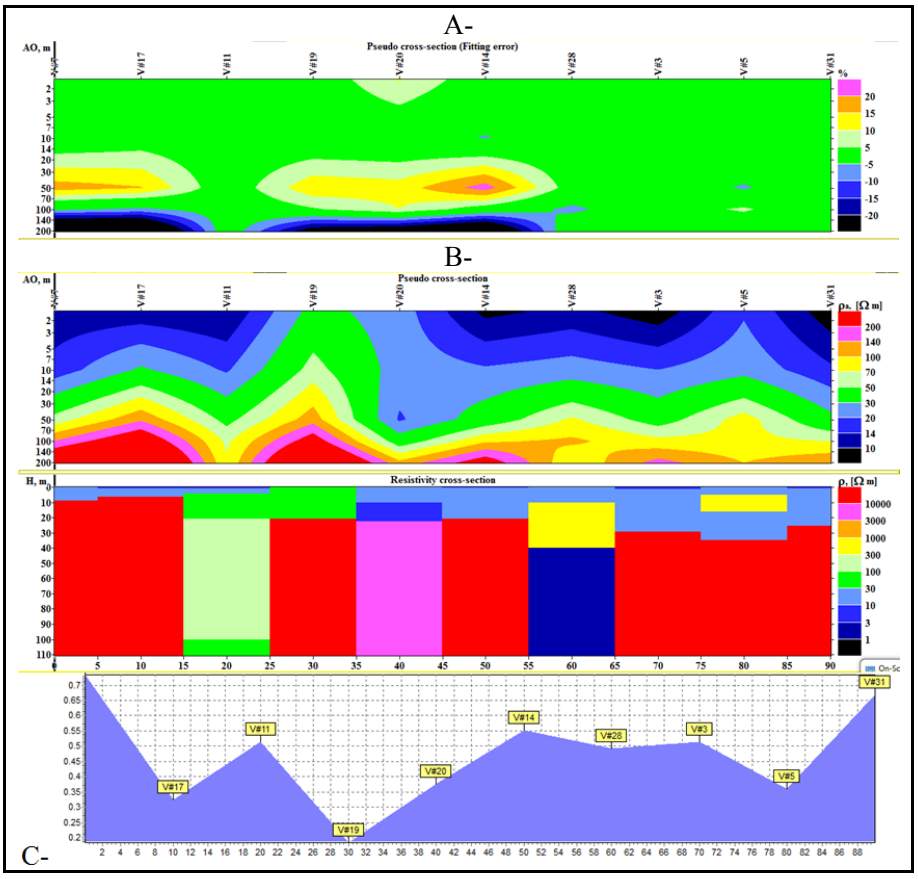

Fig. 6: Qualitative assessment of the first profile.

Figure (7) shows some analogy in its interpretation with sections in Figure (6). But, it is dominated by more sediment thickness of lower resistivity than its underlying bedrock. Much higher conductance values were detected below the VES's 39 and 22.

The simple qualitative interpretation of the studied VES's is followed by their quantative interpretation, which started with a simple interpretation using multi-layer computer program (Zohdy and Bisdorf, 1989) through an automatic interpretation giving a preliminary model that was fed into another (RES2DINV) software for better results.

So, the apparent resistivity distribution of the subsurface structure is then inverted using the commercial RES2DINV software to estimate the true resistivity structure. The algorithm uses a 2D smoothness constrained, least-squares inversion with a Jacobian matrix calculation for the first iteration and then employs a quasi-Newtonian technique to reduce numerical calculations (Loke and Barker, 1995, 1996). The inversion is stopped once the difference of the root mean square (RMS) error between the current and previous iterations is<0.1%. The inverted data produce the 2D resistivity distribution map, which can then be used for extracting information about the contactbetween sediment and bedrock (Hsu, 2010).

For each VES, an estimate of each unit's resistivity and thickness was obtained which served as starting points for estimating the thickness of the sediment overburden underneath each VES, and hence the depth to the below-lying bedrock.The interpreted results of the measured VES's are summarized in Table (1).

Table 1: Interpretation of the studied VES's in terms of number of units, their interpreted resistivity and thickness

VES#▶	VES#1		VES#2		VES#3		VES#4		VES#5	
Unit	ρ (Ohm.m)	h (m)	ρ (Ohm.m)	h (m)	ρ (Ohm.m)	h (m)	ρ (Ohm.m)	h (m)	ρ (Ohm.m)	h (m)
1	43	21	18	5	7	1	14	2	19	2
2	24	19	28	39	26	28	5	3	11	32
3	1775		3254		1432		2531		1226	
VES#▶	VES#6		VES#7		VES#8		VES#9		VES#10	
Unit	ρ (Ohm.m)	h (m)	ρ (Ohm.m)	h (m)	ρ (Ohm.m)	h (m)	ρ (Ohm.m)	h (m)	ρ (Ohm.m)	h (m)
1	11	1	11	1	22	2	37	1	23	1
2	19	3	13	8	27	6	28	7	32	6
3	33	5	1988		1708		1608		26	64
4	1439								4271	
VES#▶	VES#11		VES#12		VES#13		VES#14		VES#15	
Unit	ρ (Ohm.m)	h (m)	ρ (Ohm.m)	h (m)	ρ (Ohm.m)	h (m)	ρ (Ohm.m)	h (m)	ρ (Ohm.m)	h (m)
1	9	1	5	1	34	1	4	1	27	2
2	15	3	14	3	4	2	22	20	41	8
3	31	17	37	5	2418		1627		1247	
4	1387		2477							
VES#▶	VES#16		VES#17		VES#18		VES#19		VES#20	
Unit	ρ (Ohm.m)	h (m)	ρ (Ohm.m)	h (m)	ρ (Ohm.m)	h (m)	ρ (Ohm.m)	h (m)	ρ (Ohm.m)	h (m)
1	12	2	5	1	71	1	10	1	27	10
2	38	8	92	3	27	27	21	1	6	12
3	97	11	1691		2581		10	4	1682	
4	411						1454			
VES#▶	VES#21		VES#22		VES#23		VES#24		VES#25	
Unit	ρ (Ohm.m)	h (m)	ρ (Ohm.m)	h (m)	ρ (Ohm.m)	h (m)	ρ (Ohm.m)	h (m)	ρ (Ohm.m)	h (m)
1	32	3	22	1	4	1	7	1	75	1
2	15	26	10	11	25	23	26	28	19	12
3	1412		1665		1446		1432		2703	
VES#▶	VES#26		VES#27		VES#28		VES#29		VES#30	
Unit	ρ (Ohm.m)	h (m)	ρ (Ohm.m)	h (m)	ρ (Ohm.m)	h (m)	ρ (Ohm.m)	h (m)	ρ (Ohm.m)	h (m)
1	14	1	76	1	10	1	57	1	33	2
2	59	7	33	10	24	9	10	3	24	45
3	2433		2506		1434		35	69	1331	
4							1079			
VES#▶	VES#31		VES#32		VES#33		VES#34		VES#35	
Unit	ρ (Ohm.m)	h (m)	ρ (Ohm.m)	h (m)	ρ (Ohm.m)	h (m)	ρ (Ohm.m)	h (m)	ρ (Ohm.m)	h (m)
1	7	1	56	7	19	15	9	1	38	1
2	13	3	16	22	7	11	48	1	13	20
3	20	22	1558		1665		7	8	1331	
4	1867						1665			
VES#▶	VES#36		VES#37		VES#38		VES#39		VES#40	
Unit	ρ (Ohm.m)	h (m)	ρ (Ohm.m)	h (m)	ρ (Ohm.m)	h (m)	ρ (Ohm.m)	h (m)	ρ (Ohm.m)	h (m)
1	20	2	43	21	10	1	10	3	7	1
2	31	6	24	19	16	3	17	9	33	3
3	26	29	1775		29	17	82	57	73	18
4	1281				1861		1255		1274	

From the above deduced interpreted resistivity and thickness results, the calculated depth to the bedrock was calculated and mapped as shown in Fig. 8.

The interpreted depths range from about five meters at the fringes of the valley (Wadi Allaqi); to about sixty to seventy meters along the course of the main valley, with varying depths in between. Three deeper localized spots or depressions were reognized near the locations labeled X, Y, and Z, with depths of about

50-60 meters below the earth's surface. These localities are considered potential spots for drilling and groundwater withdrawal.

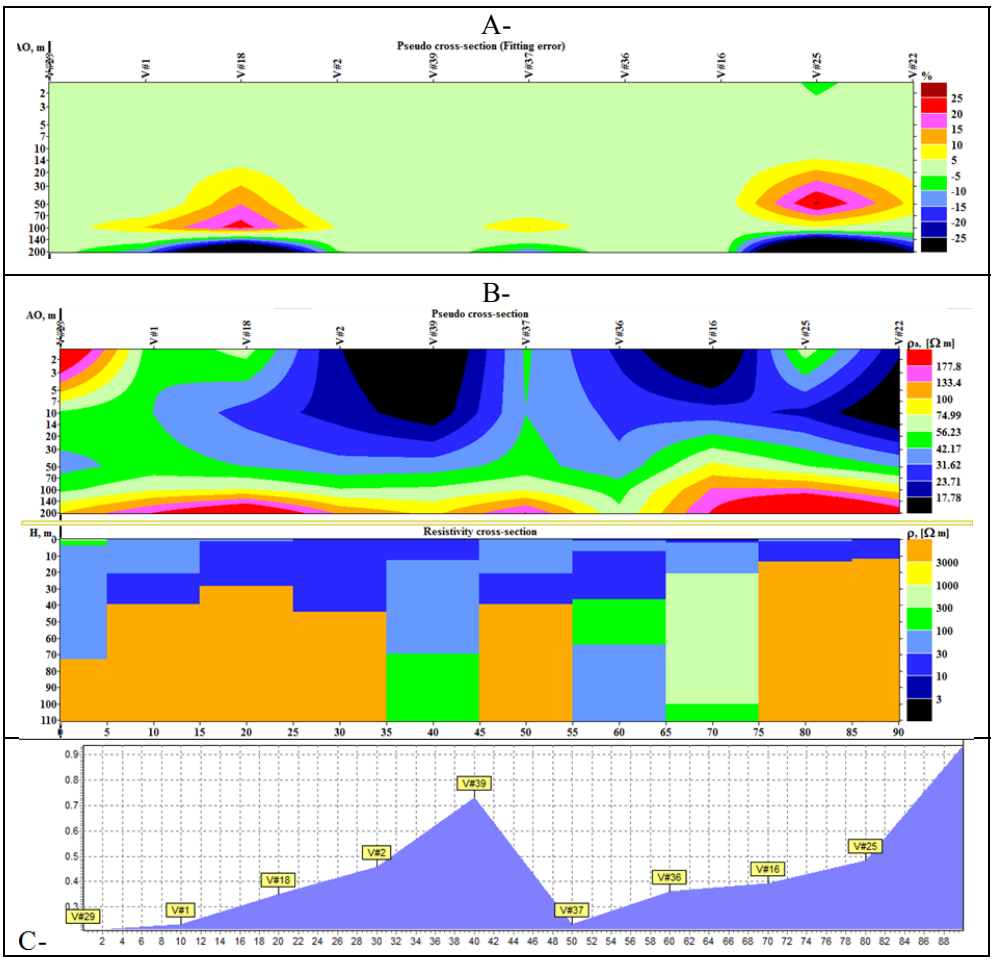

Fig. 7: Qualitative assessment of the second profile.

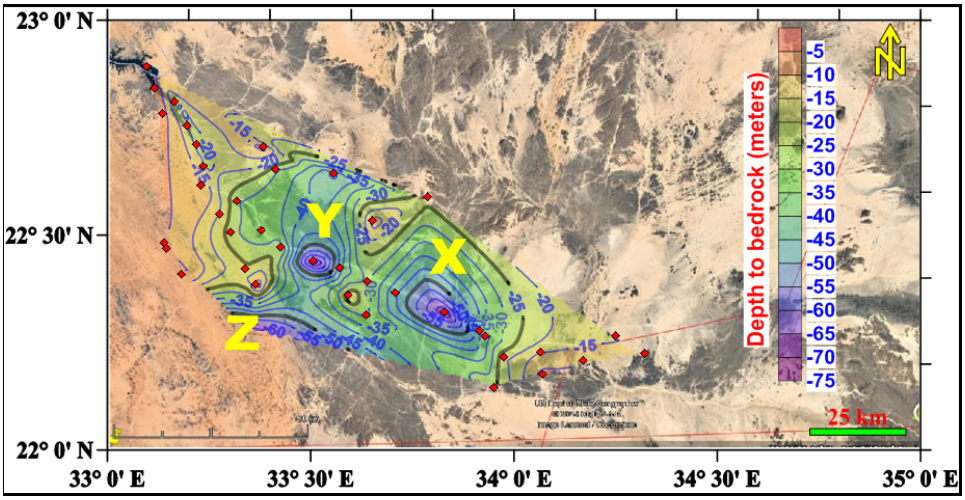

Fig. 8: Depth to the bedrock as deduced from resistivity interpretation (C.I. = 5 m)

Figure (9) illustrates a cross-sectional view for the bedrock topography as deduced from the geoelectrical resistivity analysis Figure (8) along the pathway/course of the main valley (Wadi Allaqi).

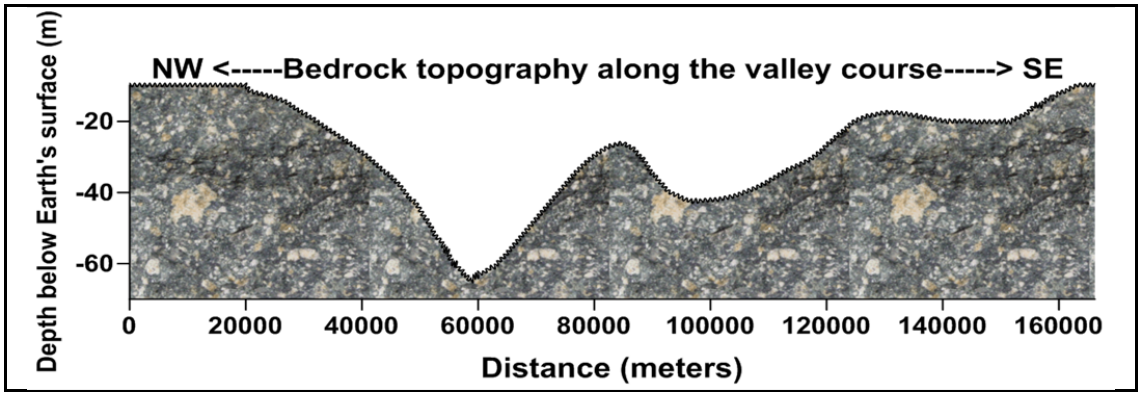

Fig. 9: Shows the bedrock topography as deduced from resistivity interpretation

From the hydrogeological perspective for the overburden lying above the bedrock, Figure (10) illustrates the weighted interpreted true resistivity for the shallower aquiferous horizon overlying the more resistant below-lying bedrock. The areas marked with symbols A and B represent areas of higher resitivity and consequently less conductive zones. May be due to harder subsurface unfractured bedrock.

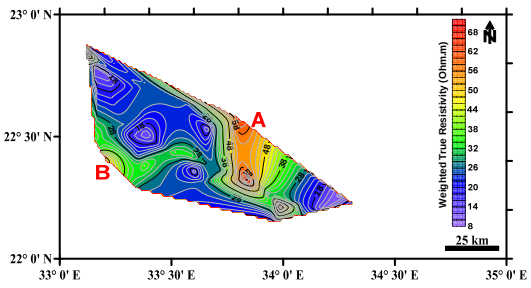

Fig. 10: Weighted true resistivity of the aquiferous unit (C.I. = 2 Ohm.m)

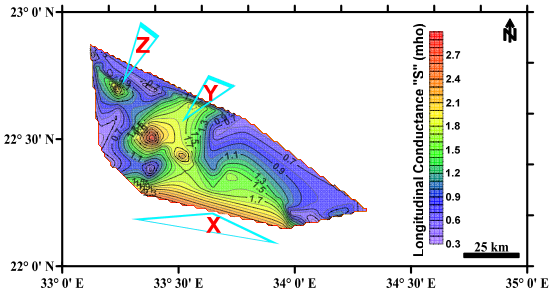

Fig. 11: Longitudinal Conductance (S) map C.I. = 0.1 mho

Hydrogeophysical (Dar Zarrouk) Parameters: Longitudinal conductance "S"

Longitudinal conductance (S): The sum of all the thickness/resistivity ratios of n −1 layers which overlie a semi-infinite substratum of resistivity ρ_n, such that $\mathbf{S} = h_1/\rho_1 + h_2/\rho_2 + h_3/\rho_3 + \ldots + h_{n-1}/\rho_{n-1}$ (mho), where h_1, h_2, etc. are the depths and ρ_1, ρ_2, etc. the resistivities, of successive layers. A knowledge of h_i/ρ_i for the ith layer when it is sandwiched between two layers of much higher resistivity is of importance in resolving the problem of equivalence.

Correlation between "**S**" and the hydrogeological potentials of the weathered, presumably aquiferous, units overlying the bedrock shows higher values of "**S**"to greater thickness of such upper fragmented weathered unit overlying the more resistant bedrock. Lower "**S**" values are linked to resistant substrata of shallower altitude that are closer to the surface. Longitudinal conductance map of the layer under consideration is given in Figure (11).

This map indicates a good conducting zone, of higher **S** (2.1-3.0 mho), along the southern part trending NWfor about 50 kilometers (labeled "**X**"), and also at the areas marked Y & Z. That may indicate possible concentration of more conductive materials in the area. Intermediate conductance (1.2-2.0 mho) contour levels striking NW may constitute an area with increased weathered basement materials. Lower conductivity values (0.3-1.1 mho) which dominate the eastern and western zones may be associated to the presence of fine grained matrix in coarse grained fractions and/or fractured bedrock where the degree of decomposition of the rock fragment is minimal.

GENERAL GRAVITY STUDY

Gravity methods play very important role in configuring the bedrock topography and subsequent groundwater exploration in certain geologic situations. It has the advantage that it is quick, inexpensive and non-destructive to the environment. This is based on the vertical and enoughlateraldensity variations

within the studied subsurface sequence. Groundwater may find its way to be accumulated within the sands and gravels in buried stream valleys and abandoned old buried river channels; underlain by massive bedrock.Buried stream valleys (Figure 12) onthe bedrock surface often contain sands andgravels and/or weathered products from the surrounding rocks or the underlying bedrock, which can be excellent reservoirs ofgroundwater.Gravity data analysis can be used to enhance the applicability of this method for this goal through converting the gravity anomalies to bedrock elevations illustrating its relief and mapping; where such bedrock troughs can be focal points for accumulating large volumes of groundwater because their porosity and permeability are usually good enough to be groundwater reservoirs.

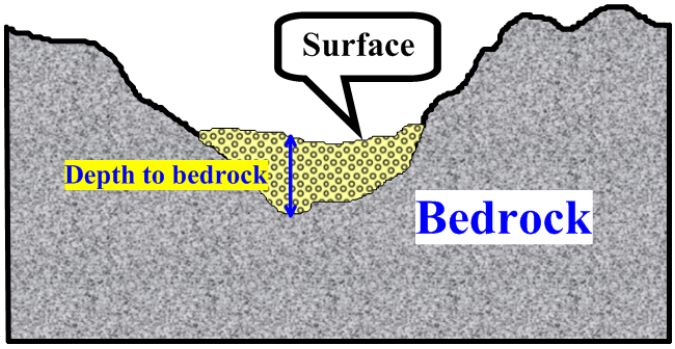

Fig. 12: Schematic cross-section of buried valley on bedrock surface

The use of Gravity method for this target requires highly resolved gravity anomalies. Therefore, this work will try to maximize the resolution of the obtained gravity data and dealing with tiny and small gravity variations as will be discussed.

The available Bouguer gravity data for the current study is illustrated in Figure (13). It shows that there are two major distinctive gravity anomalies. One major positive gravity anomaly refers to the eastern and northeastern sides of the area, while the other major negative gravity anomaly to the western and southwestern zones of the study area. The positive gravity anomaly corresponds to the outcropped crystalline volcanics and metasediments composing the exposed basement rocky terrain. While, the negative anomaly is due to the subsurface and deeper basement rocks composing the bedrock for the overlying overburden composed of sands, silts, and gravels filling the subsided section of the basement terrain. This negative anomaly coincides with the relief of Wadi Allaqi and its surrounding areas, which is the main goal of the current study.

Fig.13: Bouguer gravity map (C.I. = 5 m.Gal)

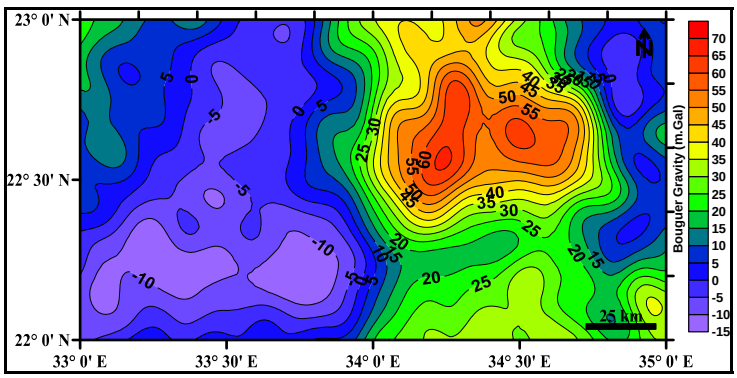

The polynomial separation method was used to produce the first and second degree regional, and consequently the corresponding residual maps. The algorithm by (Murthy and Krisshnamacharyulu, 1990) and (Gupta, 1983) was used to adjust the polynomial surfaces to the Bouguer anomaly map as exampled by (Gobashy, 2000).

This method is based on the analytical least square method and the polynomial decomposition series.The least-square method was used to compute the mathematical surface which gave the best fits to the gravity field within specific limits. This surface is considered to be the regional gravity anomaly. The residual was obtained by subtracting the regional field from the observed gravity field.

In practice, the regional surface is considered as a two-dimensional polynomial. The order of this polynomial depends on the complexity of the geology in the study area. The first, second polynomial surfaces of the regional anomaly obtained in this work is presented in (Figures 14 and 15), and the corresponding residual anomaly is presented in Figure (16).

The qualitative interpretation is based on the geophysical information that can be extracted from the deduced residual anomaly map and its relationship with the geology of the region. The main features of the residual anomaly map (Figure 16) are very similar to those of the Bouguer anomaly map (Figure 13), which represents the resulting effects of the near surface and deeper geological units within the survey area.

The residual anomaly map (Figure 16) obtained after polynomial separation portrays positive and negative values, where the positive anomaly may indicate the uplifted basement at eastern side. The residual anomalies found in the area are of different irregular shapes, but most likely trending N-S, or NNW-SSE; they are accompanied by a steeper gradient, which can be associated with structural dipping geological boundaries.

This residual anomaly map is supposed to subject to more use for delineating the subsurface bedrock relief based on the varying proposed density contrast, which will be explained later in this work. But, since the deduced residual map (Figure 16) does not reflect the needed detailed picture of the residual density variations within the main valley (Wadi Allaqi), detailed investigations was required, as will be explained in the upcoming section.

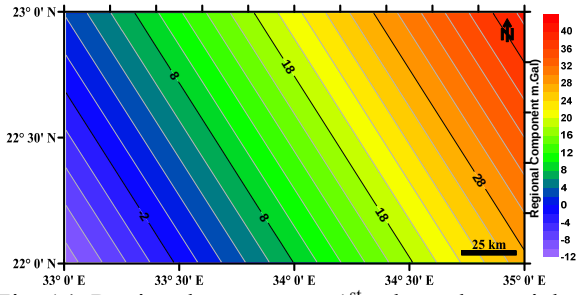

Fig. 14: Regional component 1st order polynomial (C.I.= 2 m.Gal)

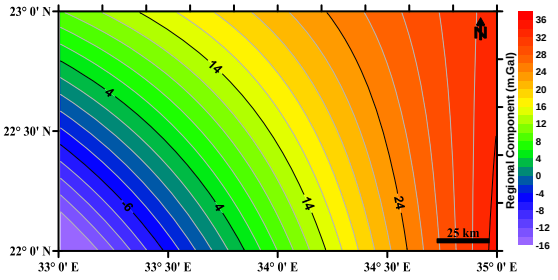

Fig. 15: Regional component 2nd order polynomial(C.I.= 2 m.Gal)

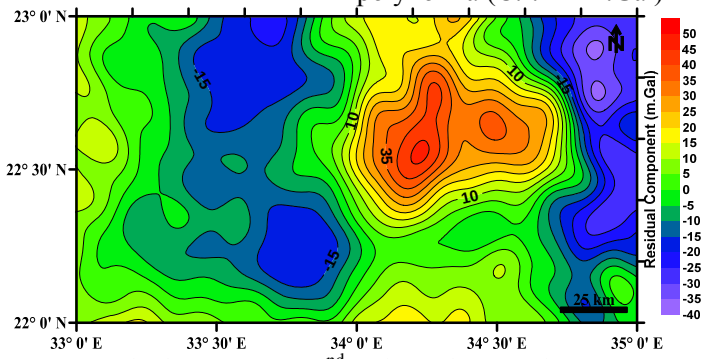

Fig. 16: Residual component 2nd order polynomial (C.I.= 2 m.Gal)

DETAILED GRAVITY STUDY

Since, the main target of the current study is to delineate the sediment thickness within Wadi Allaqi area, the low-lying valley zone within Wadi Allaqi region was further subjected to detailed gravity study through twenty profiles taken across the Bouguer anomaly in Figure (14) which coincides with Wadi Allaqi as shown in Figure (17).Ten almost northing, profiles and ten easting profiles were further investigated. The ten northing profiles are symbolled from A through J, and the ten easting profiles are symbolled from K through T. The profiles have different lengths depending on the negative anomaly coverage (which represents the underneath valley bottom) along each profile. That is why, they were taken such that to cover the low-lying western negative anomaly which is located within Wadi Allaqi region.

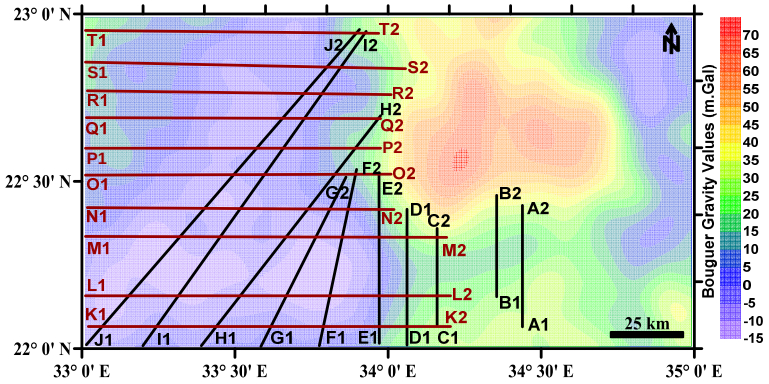

Fig. 17: Bouguer gravity anomaly map with profiles

The work on each of these profiles involved the detailed digitization of each profile at 50 meters distance intervals. For example, Profile A1-A2 is about 39.5 kms in length. Such 39.5 kilometers were digitized into 790 points/dots at 50 meters intervals. The produced dots, *which represent stationed-gravity values*, were then subjected to further detailed separation into their regional and residual components using Griffen method (1949). Such detailed regional and residual components are definitely different than the general regional and residual components deduced from Figures (14, 15 and16) by polynomial technique. This procedure was implemented on all the studied profiles' data. The deduced regional and residual components' data were then contoured and mapped, as shown in Figures (18) and (19), respectively.

The obtained detailed residual gravity data were then subjected to the required quantitative interpretation to estimate the thickness of the infilling sediments or alluvium which represents the areal extension of the explorable groundwater aquifer within Wadi Allaqi region.

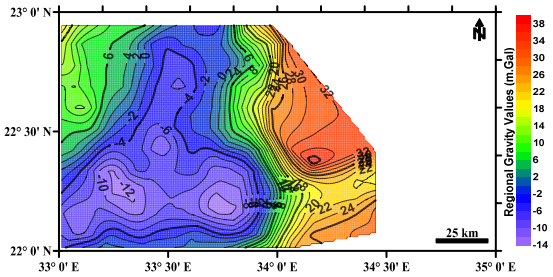

Fig. 18: Detailed regional Gravity (C.I. = 2 m.Gal)

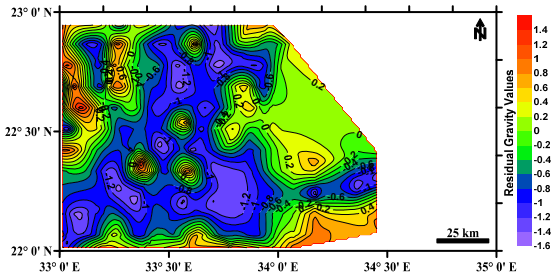

Fig. 19: Detailed residual Gravity (C.I. = 0.2 m.Gal)

The technique used in evaluating the thickness of the Wadi infilling material which corresponds to the depth to the underlying basement bedrock is explained as follows.

It is well-known that the main factors affecting the gravity anomaly magnitude are the depth to the subsurface causative feature and the density contrast. This is based on the following equation (Van Overmeeren, 1975):

$$\Delta h = \Delta g / (2\pi G.\Delta\rho)$$

Where "Δh" is the depth to the causative feature, "Δg" is the residual gravity value, and "$\Delta\rho$" is the density contrast. So, using a proper value for the density contrast together with obtained detailed residual gravity value, the depth can be estimated.

Therefore, in the current study, a chart illustrating the relation between the magnitude of the detailed residual gravity anomaly at variable density contrasts and bedrock depths was developed, as shown in Figure (20).

Usually, the density of the silts, sands, gravels and weathered debris (in general) overlying and infilling the bedrock troughs have a range of density of about 1.9-2.3 gm/cm^3. While, knowing the lithological composition of the bedrock and their surrounding exposed/outcropped counterpart's rocks, it is found that

their density range is about 2.3-2.7 gm/cm^3. Based on using a proper density contrast between the valley infillings and the adjacent bedrock; this will give a local gravity low over the valley, assuming uniform lateral density. It can be concluded that the density contrast range in our case is ranging between 0.1 to 1.0 gm/cm^3.

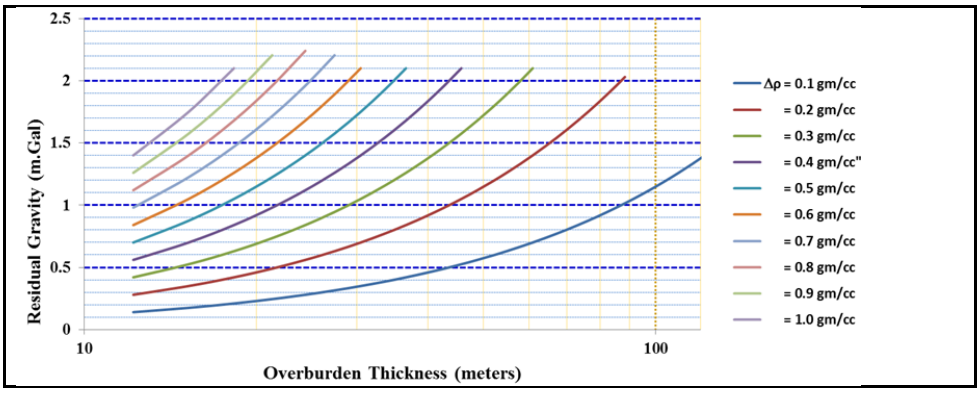

Fig. 20: Relation between overburden thickness and residual gravity at various density contrasts

Accordingly, applying the relation mentioned above on every residual gravity value as obtained from Figure (19) along each profile at various density contrast values, tremendous amount of results were obtained, which exemplified in Table (2). The same procedure was carried out with all the studied profiles. The depth results were mapped giving the same anomaly shapes, but with varying depth values.

Table 2: Part of the estimated depth values at discrete point intervals along profile (A1-A2) at varying density contrasts

Den. Con=0.1	Den. Con=0.2	Den. Con=0.3	Den. Con=0.4	Den. Con=0.5	Den. Con=0.6	Den. Con=0.7	Den. Con=0.8	Den. Con=0.9	Den. Con=1.0
55.91	27.95	18.64	13.98	11.18	9.32	7.99	6.99	6.21	5.59
54.86	27.43	18.29	13.72	10.97	9.14	7.84	6.86	6.10	5.49
54.32	27.16	18.11	13.58	10.86	9.05	7.76	6.79	6.04	5.43
59.59	29.80	19.86	14.90	11.92	9.93	8.51	7.45	6.62	5.96
67.18	33.59	22.39	16.79	13.44	11.20	9.60	8.40	7.46	6.72
77.93	38.97	25.98	19.48	15.59	12.99	11.13	9.74	8.66	7.79
86.21	43.10	28.74	21.55	17.24	14.37	12.32	10.78	9.58	8.62
85.63	42.82	28.54	21.41	17.13	14.27	12.23	10.70	9.51	8.56
83.91	41.95	27.97	20.98	16.78	13.98	11.99	10.49	9.32	8.39
90.19	45.10	30.06	22.55	18.04	15.03	12.88	11.27	10.02	9.02
88.45	44.23	29.48	22.11	17.69	14.74	12.64	11.06	9.83	8.85
85.06	42.53	28.35	21.27	17.01	14.18	12.15	10.63	9.45	8.51
81.03	40.51	27.01	20.26	16.21	13.50	11.58	10.13	9.00	8.10
74.85	37.42	24.95	18.71	14.97	12.47	10.69	9.36	8.32	7.48
70.26	35.13	23.42	17.57	14.05	11.71	10.04	8.78	7.81	7.03
67.41	33.71	22.47	16.85	13.48	11.24	9.63	8.43	7.49	6.74
65.34	32.67	21.78	16.34	13.07	10.89	9.33	8.17	7.26	6.53
65.52	32.76	21.84	16.38	13.10	10.92	9.36	8.19	7.28	6.55
65.47	32.74	21.82	16.37	13.09	10.91	9.35	8.18	7.27	6.55
63.86	31.93	21.29	15.97	12.77	10.64	9.12	7.98	7.10	6.39
62.37	31.19	20.79	15.59	12.47	10.40	8.91	7.80	6.93	6.24
60.88	30.44	20.29	15.22	12.18	10.15	8.70	7.61	6.76	6.09
59.48	29.74	19.83	14.87	11.90	9.91	8.50	7.43	6.61	5.95
…..	…..	…..	…..	…..	…..	…..	…..	…..	…..

Then, based on the results obtained from the geoelectrical resistivity analysis in the current study where the maximum obtained depth to the bedrock at specific comparable locations was about 60 to 70 meters along the course of the valley (Wadi Allaqi), it is concluded that the closest depth results from the gravity analysis to the obtained resistivity analysis are the ones which was computed using the density contrast of 0.2 gm/cm^3. So, the depth results obtained from the detailed residual gravity analysis using density contrast of 0.2 gm/cm^3 were mapped to illustrate the varying depths to the underlying bedrock as shown in Figure (21).

Overall, there is very close approximation between the bedrock topography obtained from the resistivity analysis to the one obtained from the detailed residual gravity analysis, in general. But, the bedrock relief obtained from gravity analysis is covering larger zones within the study area with more detailed localized depths than obtained from the resistivity analysis.

Figure (22) shows the configuration of the bedrock surface as deduced from the quantitative interpretation of the detailed residual results of Bouguer gravity data along the valley (Wadi Allaqi) course, represented by the dotted line in Figure (21). This configuration illuminates more detailed bedrock relief with higher resolution than that one deduced from resistivity interpretation (Figure 9). That is because in case of using the gravity data, the used station spacing was small enough(50 m) to produce much more resolved picture about the bedrock surface variations, while in case of using the resistivity data, the spacing between the studied VES's locations was large enough (10's of kilometers) to provide smoother configuration.

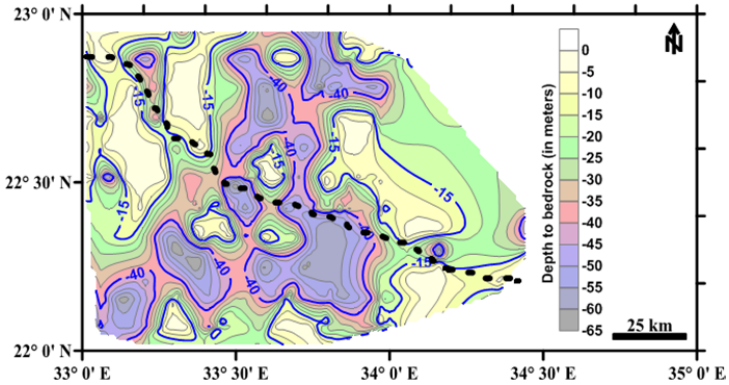

Fig. 21: The topography of the bedrock relief within Wadi Allaqi and surrounding areas as deduced from the detailed residual gravity analysis (the dotted line shows the valley course)

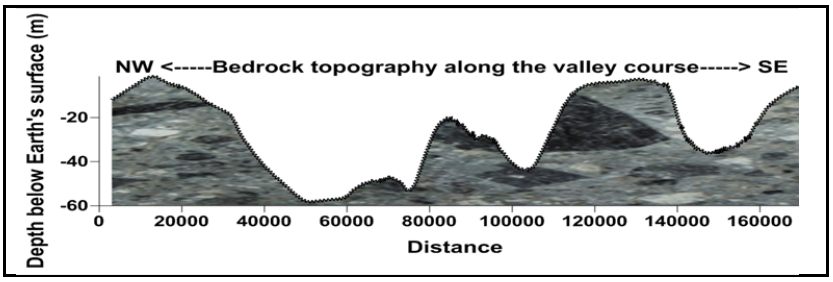

Fig. 22: Bedrock topography as deduced from gravity interpretation

Another cross-sectional view (Figure (23)) was taken along the longest studied gravity profile (J1-J2) shown in Figure (17) to illustrate the estimated overburden thickness variations as deduced from the gravity data detailed interpretation on a more lengthy scale. It shows that the overburden thickness is getting thinner at the peripheries of Wadi Allaqi due to the uprising of the basement bedrock around it. While the overburden shows relatively more thickness at the far southwestern zone of the study area with the probable presence of another depression to the southwest of Wadi Allaqi along the direction of this studied J1-J2 profile.

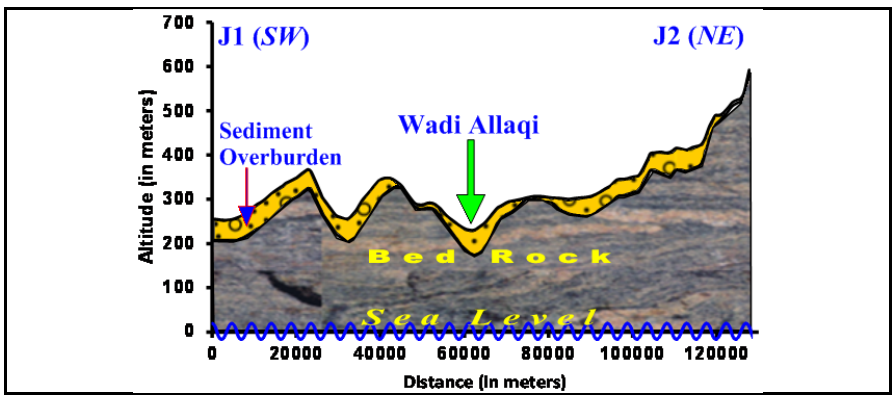

Fig. 23: Cross-sectional view showing the altitude variations of elevation, bedrock topography, and thickness variations along the Profile J1-J2

CONCLUSIONS

Geophysical field measurements in terms of vertical electrical resistivity surveying and Bouguergravity data were studied at Wadi Allaqi area, Eastern Desert, Egypt; aiming at acquiring an idea about the configuration of the bedrock (basement) surface, and assessing the groundwater potentiality and the best locations for drilling groundwater boreholes.

Smoothed imaging of the bedrock releif was deduced from resisivity interpretation due to the wider spacing between the studied VES's locations, while a more resolved picture with more details of the bedrock surface variations was inferred from the detailed residual results of Bouguer gravity datainterpretation due to the more dense station spacings between gridded residual gravity data.

Three main deeper depressions with varying extensions considered as best locations for groundwater accumulation and suitable for drilling of groundwater boreholes were found.

REFERENCES

Dahlin, T., Jens, E., Dowen, R., Mangeya, P., Auken, E., (1999): Geophysical andhydrogeologic investigation of groundwater in the Karoo stratigraphic sequenceat Sawmills in northern Matabeleland, Zimbabwe: a case history. Hydrogeol. J.15 (5), 945–960.

El-Shazly, M. E. (1964): On the classification of the Precambrian and other rocks of magmatic affiliation in Egypt. Ann. Geol. Surv. Egypt IV, 125–135.

Gobashy, M. M. (2000): Basin Evaluation from Gravity Measurements using Simplex Algorithm with Application from Sirt Basin, Libya. Bulletin of Faculty of Science, Zagazig University, 22, 62-80.

Gupta, V. K. (1983): A Least Squares Approach to Depth Determination from Gravity Data. Geophysics, 48, 357-360. https://doi.org/10.1190/1.1441473.

Hanaa A. Kandal & Hoda A. Yacoub & Menno P. Gerkema & Jac. A. A. Swart (2016): Vanishing Knowledge of Plant Species in the Wadi Allaqi Desert Area of Egypt. Hum Ecol, 44, 493–504.

Han-Lun Hsu, Brian J. Yanites, Chien-chih Chen, Yue-Gau Chen (2010): Bedrock detection using 2D electrical resistivity imaging along the Peikang River, central Taiwan. Geomorphology 114,.406–414.

Kearey, P., Brooks, M., (1991): An Introduction to Geophysical Exploration, 2nd Edition. Blackwell Scientific, Oxford Publishing House.

Khedr E.S., Youssef A. A. E., Abou Elmagd K., Khozyem H. M.(2010): Tectono-stratigraphic subdivision of the clastic sequence of Aswan area, southern Egypt. Fifth International Conference on the Geology of the Tethys Realm, South Valley University, January 2010, P. 197-216.

Keller, G. V., Frischknecht, F. C., (1966): Electrical Methods in Geophysical Prospecting.Pergamon, Oxford, UK.

Loke, M. H., Barker, R. D., (1995): Least-squares deconvolution of apparent resistivity pseudosections. Geophysics 60, 1682–1690.

Loke, M.H., Barker, R.D., (1996): Rapid least-squares inversion of apparent resistivity pseudosections by a quasi-Newton method. Geophys. Prospect. 44, 131–152.

Meju, M., (2005): Simple relative space–time scaling of electrical and electromagnetic depthsounding arrays: implications for electrical static shift removal and joint DC TEM datainversion with the most-squares criterion.Geophys.Prospect. 53, 1–17.

Metwaly, M., El-Qady, G., Massoud, U., El-Kenawy, A., Matsushima, J., Al-Arifi, N., (2009): Integrated geoelectrical survey for groundwater and shallow subsurface evaluation: case study at Siliyin spring, El-Fayoum, Egypt. Int. J. Earth Sci. 99, 1427–1436.

Murthy, I.V.R. and Krisshnamacharyulu, S.K.G. (1990): A Fortran 77 Programme to Fit a Polynomial of Any Order to Potential Field Anomalies. J. Assoc. Explor. Geophys., 11, 99-105.

Ndlovu, S., Mpofu, V., Manatsa, D., Muchuweni, E., (2010): Mapping groundwater aquifers using dowsing, slingram electromagnetic survey method and vertical electrical sounding jointly in the granite rock formation: a case of Matshetshe.

Nowroozi, A. A., Horrocks, S. B., Henderson, P., (1999): Saltwater intrusion into the fresh water aquifer in the eastern shore of Virginia: a reconnaissance electrical resistivity survey. J. Appl. Geophys. 42, 1–22.

Olayinka, A. I., (1991): Geophysical siting of boreholes in crystalline basement areas of Africa. J. Afr. Earth Sci. 14 (2), 197–207.

Shams A. M. Issa, M.A.M. Uosif and L.M. Abd-El-Salam (2012): Natural radionuclideconcentrations in Granite rocks in Aswan and central-southern Eastern Desert, Egypt and their radiological Implications. Radiation Protection Dosimetry, 150(4), 488–495.

Stern, R. J. and Hedge, C. (1985): Geochronological and isotopic constraints on late pressure crustal evolution in the Eastern Desert of Egypt. Am. J. Sci. 285, 97–172.

Stewart, M. T., (1982): Evaluation of electromagnetic methods for rapid mapping of salt water interfaces in coastal aquifers. J. Ground Water 20, 538–545.

Telford, E., Geldart, W.M., Sheriff, R.E., (1990): Applied Geophysics. Cambridge University Press, UK.

Van Overmeeren, R., (1989): Aquifer boundaries explored by geoelectrical measurements inthe coastal plain of Yemen. A case of equivalence. Geophysics 54, 38–48.

Van Overmeeren. R. A., 1975. A combination ofgravity and seismic refraction measurements applied to groundwater exploration near Taltal, province of Antofagasta Chile: Geophys. Prosp. 23. 248-258.

Zohdy, A. A. R., and Bisdorf, R., (1989): A program for automatic processing and interpretation of Schlumberger sounding curves in Quick Basic 4.0. U. S. Geol. Surv., Open - File Report, 89-137, 67

Zoheir B. and Emam A. (2012): Integrating geologic and satellite imagery data for high-resolution mapping and gold exploration targets in the South Eastern Desert, Egypt. Journal of African Earth Sciences 66–67 / 22–34.

Shaping buried bedrock topography using resistivity and gravity data

تشكيل طوبوغرافية صخور الأساس باستخدام بيانات المقاومة والجاذبية في وادي العلاقي بالصحراء الشرقية ، مصر

أحمد صبحي هلالي

جامعة عين شمس – كلية العلوم – قسم الجيوفيزياء

الخلاصة

تم تقييم المقاومة الكهربائية الرأسية وبيانات جاذبية بوجير في منطقة وادي العلاقي بالصحراء الشرقية ، مصر بهدف التعرف على شكل تضاريس سطح صخور القاعدة ، وإمكانية توافر أماكن تصلح لتجمع المياه الجوفية وتقييم أفضل المواقع لحفر آبار المياه الجوفية. وقد أظهرت النتائج التي تم الحصول عليها من تفسير المقاومة الجيوكهربية أن العمق المستنتج لسطح صخور القاعدة يتراوح من حوالي خمسة أمتار إلى ستين مترًا مع ثلاثة منخفضات عميقة نسبيا وتعتبر أفضل المواقع لتراكم المياه الجوفية ومناسبة لحفر آبار المياه الجوفية. وحيث أن شدة الجاذبية تعتمد بشكل رئيسي على العمق بالإضافة إلى فرق الكثافة بين الرواسب القريبة من السطح مع صخور القاعدة السفلية – تم إجراء العديد من التجارب لتقدير العمق بمختلف تباين الكثافة (٠.١-١.٠ جم/سم^{٣}).

وقد وجد أن أقرب الأعماق من تحليل الجاذبية إلى تحليل المقاومة الكهربية التي تم الحصول عليها – هي تلك التي تم حسابها باستخدام تباين الكثافة ٠.٢ gm/cm^3 كقيمة مثلى لفرق الكثافة تم إستخدامه لحاسب سمك الرواسب التي تعلو صخور القاعدة تحت السطحية.